Department of Aerospace Engineering
University of Michigan

CFD Project 3 November 2016
Ann Arbor, Michigan

Project 3: Flow over a Three-Element Airfoil

AE523, Computanial Fluid Dynamics, Fall 2016

Tzu-Hsiang Lin *

1 Introduction

In this project, the first and second-order finite volume method will be applied for solving a compressible, subsonic flow over a three-element, high-lift devices exploited airfoil. In the post-processing, the resulting forces, lift and drag coefficient, contours and streamlines will be shown.

This report is arranged as follows. The project begin in section 2 with the geometry, parameters setting and numerical methods. In section 3, the result of first-order finite volume scheme with two coarse meshes: 1149 and 2116 elements will be discussed. In section 4, second-order finite scheme will be applied on the previous meshes. In section 5, two more dense meshes, 4124 and 8031 elements, will be use for comparing the difference between first and second-order finite volume method.

2 Geometry, Parameters and Numerical Methods

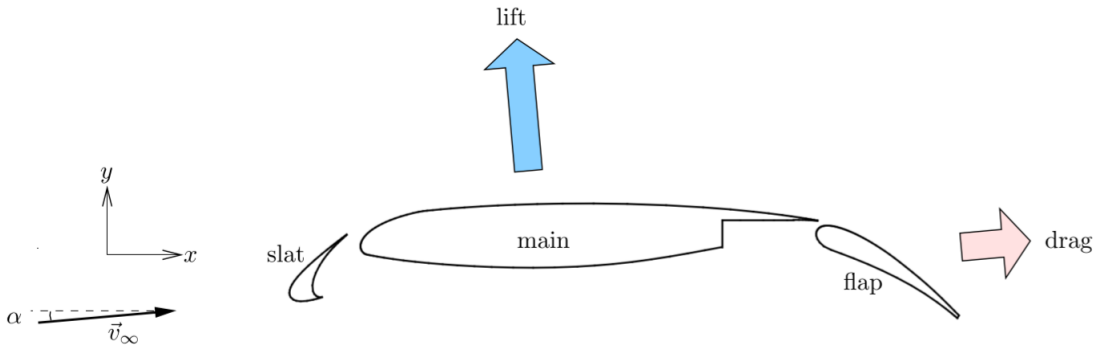

fig. 1: The initial condition of the density distribution of a traffic flow equation.

[1]email: tzuhslin@umich.edu

3 First-order Finite Volume Method

3.1 Implement a first-order finite volume method on given meshes

In the zipped files, there are five individual python files, named in *runfv2D.py*, *fv2D.py*, *mesh.py*, *flux.py* and *post.py*. For loading and processing mesh files are coded in *mesh.py*. The first-order volume method is coded in the function named *firstorderfv* in *fv2D.py* and *flux.py*. For lift and drag coefficient calculation are coded in *post.py*.

3.2 Run the codes on two meshes: mesh 0 and mesh 1

Here, mesh 0 and mesh 1 indicates the different mesh elements, 1149 and 2116 elements, respectively. To run the code, the user just need to set up the mesh type and indicates which scheme he or she wants, first-order or second-order, in *runfv2D.py* file. And the corresponding results are listed below.

3.2.1 Plot the residual and C_l convergence with iterations

Figure 2 shows how first-order finite volume scheme converge. Here, I define the criteria for convergence as when the maximum residual(L_{inf} norm) below than 10^{-7}. It is clear to see that, for mesh 1, 2116 elements, it takes more iterations than mesh 0,1149 elements, takes to converge, however, the oscillation pattern between these two meshes are still quite similar.

Similar trend can also be observe in Figure 3, C_l convergence. In lift coefficient convergence, the oscillation in mesh 0 and mesh 1 are similar before it converge. However, for denser mesh, mesh 1, the C_l is slightly higher than mesh 0. More specific lift and drag coefficient results are discussed in section 3.2.2.

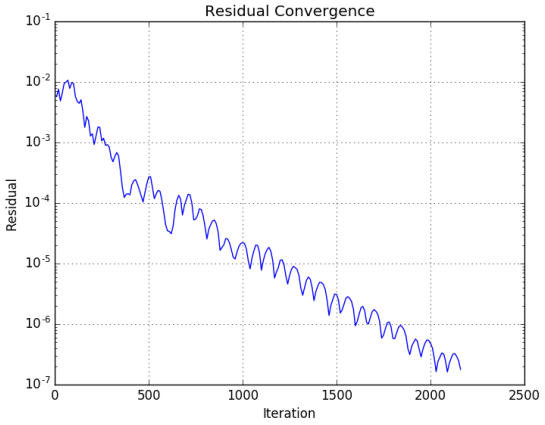

(a) Mesh 0: 1149 elements

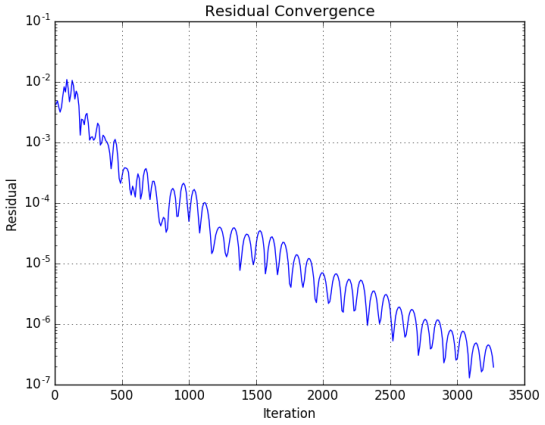

(b) Mesh 1: 2116 elements

fig. 2: Residual convergence for mesh 0 and mesh 1 with first-order finite volume method implementation.

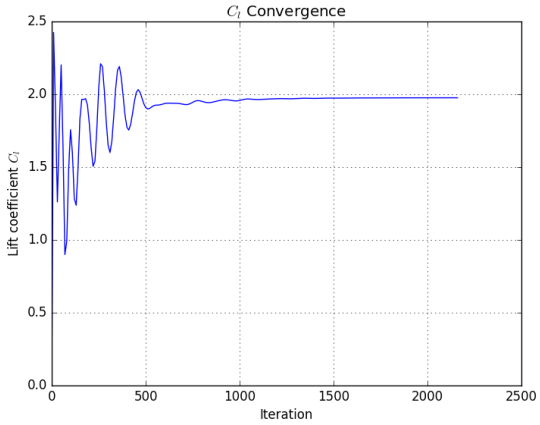

(a) Mesh 0: 1149 elements

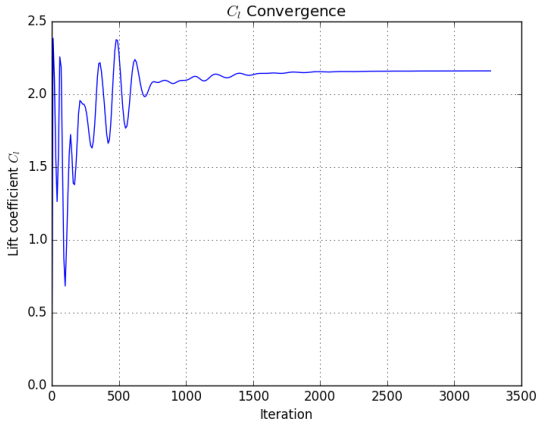

(b) Mesh 1: 2116 elements

fig. 3: Lift coefficient convergence for mesh 0 and mesh 1 with first-order finite volume method implementation.

3.2.2 The total C_l and C_d values

(a) mesh 0: 1149 elements

	total	main	slat	flap
C_l	1.9761	1.5261	0.0078	0.4422
C_d	0.3147	-0.0078	0.0495	0.2730

(b) mesh 1: 2116 elements

	total	main	slat	flap
C_l	2.1608	1.6670	0.0273	0.4664
C_d	0.2812	-0.03019	0.0354	0.2761

Table 1: The lift and drag coefficient for mesh 0 and mesh 1 with first-order finite volume method implementation.

In this subsection, the difference of the lift and drag coefficient between two different meshes will be discussed. Since this is an airfoil with slat and flap elements, the lift and drag coefficients contributed from each part are listed in Table 1. Table 1 indicates that the total lift coefficient of mesh 1 is slightly higher than mesh 0(roughly 0.2 difference), and for drag coefficient, mesh 1 has lower value than that of mesh 0, which leads to a more reasonable L over D value. Despite the different of total value, two meshes show that the main wing contributes the most part of the lift coefficient and, surprisingly, has negative value of drag coefficient.

3.2.3 The Mach and pressure contours

The contour of Mach number and pressure can provide us a straightful information. Form Mach number contour, shown in the Figure 4, both mesh 0 and mesh 1 show that the flow on upper surface has higher velocity than lower surface, which is under my expectation. However, for mesh 1, the high speed region is much less than that of mesh 0.

For pressure contour, shown in Figure 5, the pressure above the airfoil is less than the bottom of it, which is under expectation just like the Mach contour. However, the difference of pressure contour between mesh 0 and mesh 1 is not as clear as that of the Mach number contour.

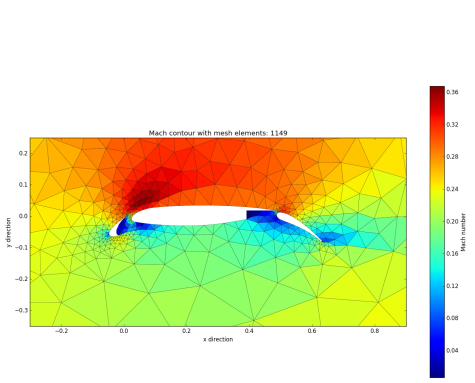

(a) Mesh 0: 1149 elements

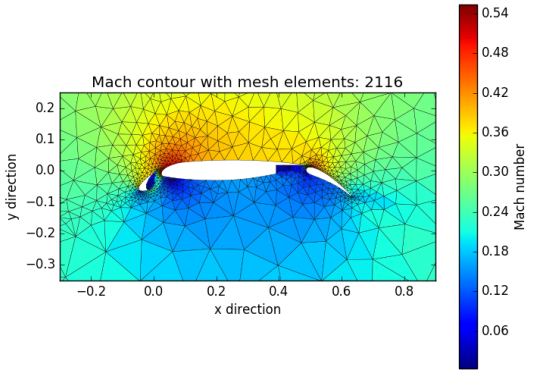

(b) Mesh 1: 2116 elements

fig. 4: Mach number contour for mesh 0 and mesh 1.

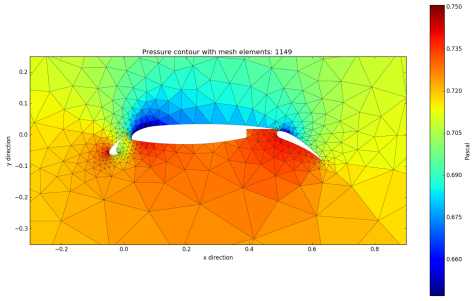

(a) Mesh 0: 1149 elements

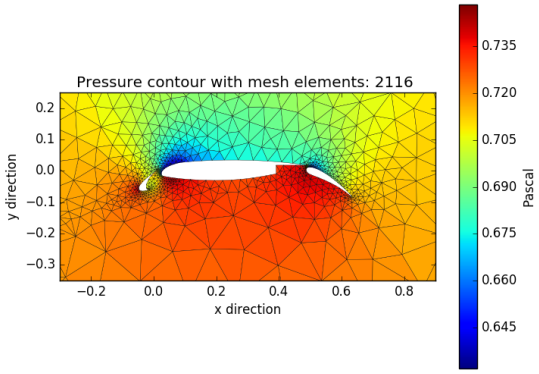

(b) Mesh 1: 2116 elements

fig. 5: Pressure contour for mesh 0 and mesh 1.

3.2.4 The surface pressure coefficient, C_p, distribution

As we know that the pressure exert on the surface of an airfoil dominates the resulted force, which leads to lift and drag. Plotting out the distribution of the pressure coefficient can make us easily understand the function of each part of an airfoil. Figure 6 indicates that the flap leads to a considerable pressure difference between upper and lower airfoil, which increases the lift on the airfoil but also momentum.

On the other hand, the slap does not contribute as much pressure difference as flap does, however, the main function for slat is try to delay the stall angle of attack but not increase lift.

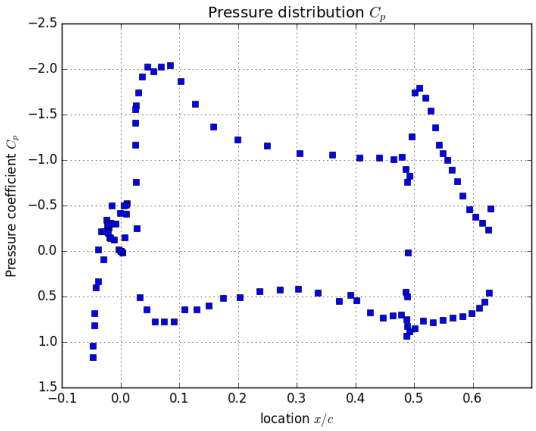

(a) Mesh 0: 1149 elements

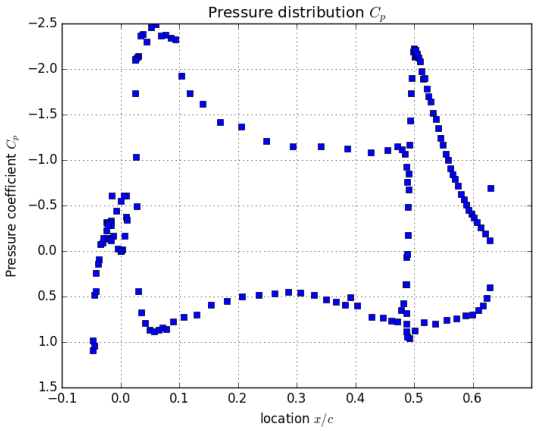

(b) Mesh 1: 2116 elements

fig. 6: Pressure Coefficient C_p contour for mesh 0 and mesh 1.

3.3 Plot the streamlines and calculate the mass flow rate in the slat/main and main/flap gaps.

Figure 7 shows how the air flows over the airfoil, and Table 2 indicates the unit mass flow rate between main/slap and main/flap gaps. Overall, both meshes share a similar streamline pattern and provide the proof that some airflow, indeed, flows through the gaps between airfoil elements, contribute the mass flow rate in Table 2.

(a) mesh 0: 1149 elements

gap location	mass flow rate
slap/main	0.003441
flap/main	0.001684

(b) mesh 1: 2116 elements

gap location	mass flow rate
slap/main	0.004054
flap/main	0.001870

Table 2: Mass flow rate between the main/slap, main/flap gaps, for mesh 0 and mesh 1.

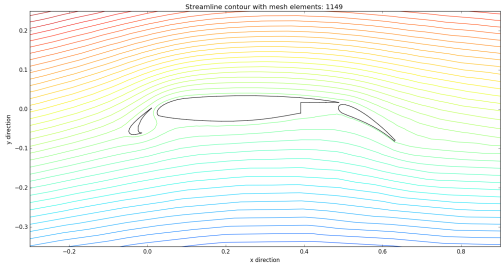

(a) Mesh 0: 1149 elements

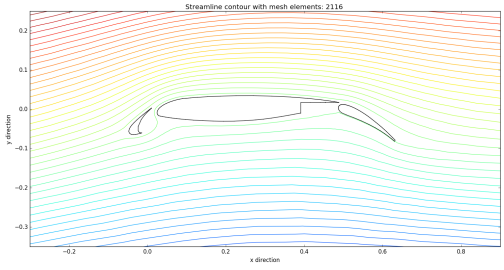

(b) Mesh 1: 2116 elements

fig. 7: Streamline contour for mesh 0 and mesh 1.

4 Second-order Finite Volume Method

4.1 Implement a first-order finite volume method on given meshes

Other than using first-order finite volume method, a second-order scheme usually provide a higher accurate solution. The corresponding codes are coded in the function named *secondorderfv* in *fv2D.py*. Same as first-order, the results from second-order scheme, such as: lift, drag and pressure coefficients, streamline, Mach number and total pressure contours, will be shown in this section.

4.2 Run the codes on two meshes: mesh 0 and mesh 1

Similarly, mesh 0 and mesh 1 will be used as the testing meshes. To implement the second-order scheme, simply set the order equal to 2 in the *runfv2D.py* file.

4.2.1 Plot the residual and C_l convergence with iterations

Figure 8 shows how second-order finite volume scheme converge. Here, I remain the criteria for convergence as when the maximum residual(L_{inf} norm) below than 10^{-7}. It is clear to see that, for mesh 1, 2116 elements, it takes about 1000 iterations more than mesh 0,1149 elements, takes to converge, however, compare to first-order, both meshes need more iteration to converge. the oscillation pattern between these two meshes are still quite similar.

Similar trend can also be observe in Figure 3, C_l convergence. In lift coefficient convergence, the oscillation in mesh 0 and mesh 1 are similar before it converge. However, for denser mesh, mesh 1, the C_l is slightly higher than mesh 0. More specific lift and drag coefficient results are discussed in section 3.2.2.

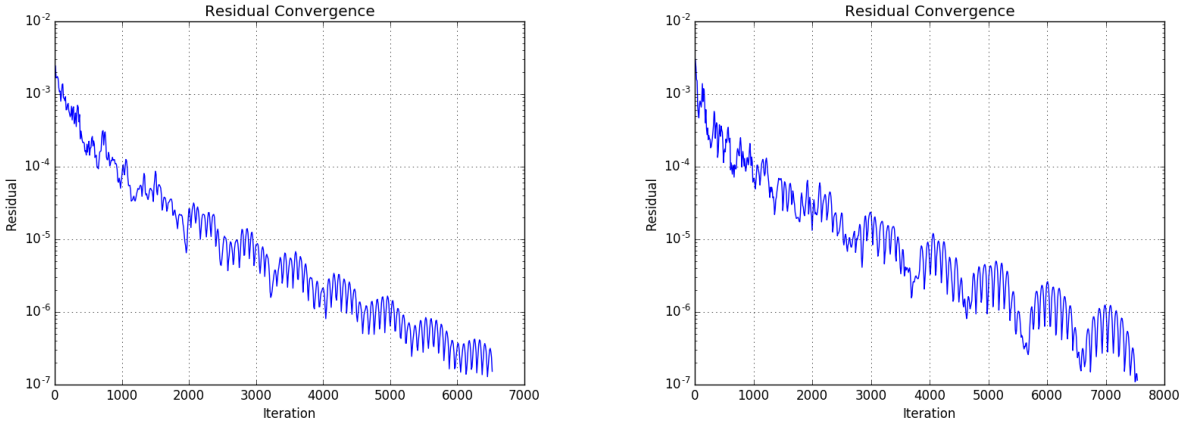

(a) Mesh 0: 1149 elements

(b) Mesh 1: 2116 elements

fig. 8: Residual convergence for mesh 0 and mesh 1 with second-order finite volume method implementation.

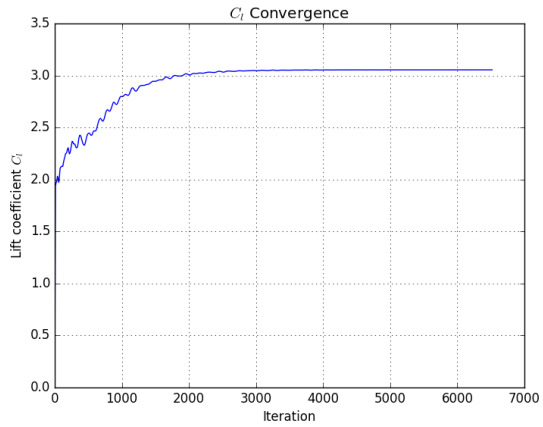

(a) Mesh 0: 1149 elements

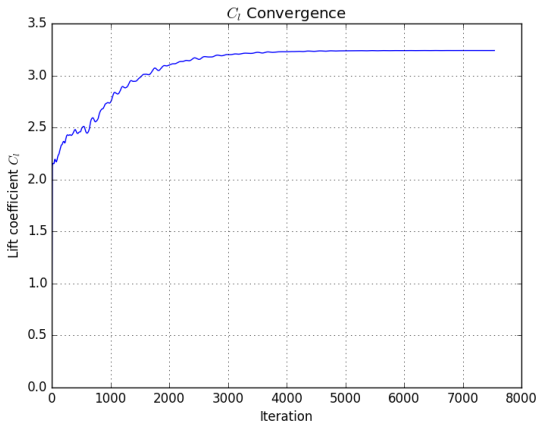

(b) Mesh 1: 2116 elements

fig. 9: Lift coefficient convergence for mesh 0 and mesh 1 with second-order finite volume method implementation.

4.2.2 The total C_l and C_d values

(a) mesh 0: 1149 elements

	total	main	slat	flap
C_l	3.0543	2.3174	0.1587	0.5781
C_d	0.06289	-0.1415	-0.1021	0.3065

(b) mesh 1: 2116 elements

	total	main	slat	flap
C_l	3.2401	2.4217	0.1811	0.6379
C_d	0.0440	-0.1558	-0.1314	0.3313

Table 3: The lift and drag coefficient for mesh 0 and mesh 1 with second-order finite volume method implementation.

The difference of the lift and drag coefficient between two different meshes, again, will be discussed in this section. Compare to first-order scheme, lift coefficient increases remarkably, peak at 3.0543 for mesh 0, 3.2401 for mesh 1. And for drag coefficient, both meshes have lower values; similarly, flap contributes the most part of the drag and slat and main elements contribute the negative drag coefficient. Overall, second-order scheme gives a higher L over D value than first-order.

4.2.3 The Mach and pressure contours

Similar to the first-order, mesh 1 tends to give a more subtle Mach number distribution around the airfoil elements. However, for these two meshes run, Mach number contours reveal that there are two accelerating points, one is at the front of the leading edge of the main part, another is the leading edge of the flap.

For pressure contour, shown in Figure 11, testify the result of the mesh contours. two low pressure regions are locating at the leading edge of main and slat elements. A very high pressure spot at the leading edge of the slat indicates the spot of stagnation point.

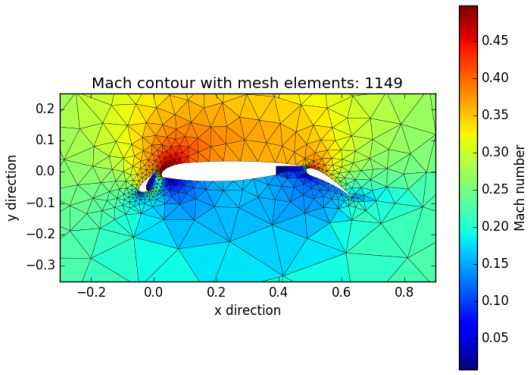

(a) Mesh 0: 1149 elements

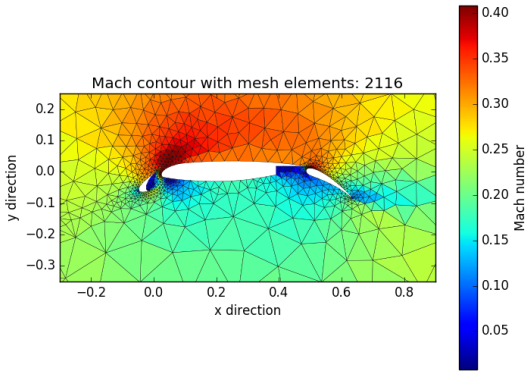

(b) Mesh 1: 2116 elements

fig. 10: Mach number contour for mesh 0 and mesh 1.

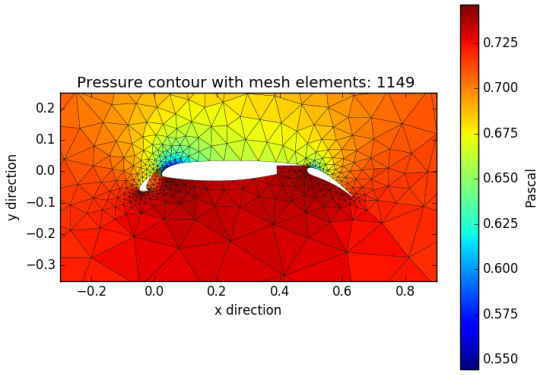

(a) Mesh 0: 1149 elements

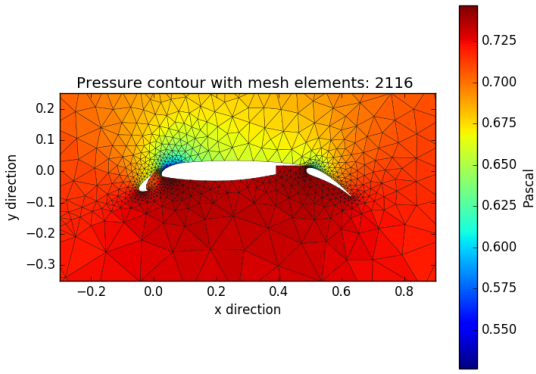

(b) Mesh 1: 2116 elements

fig. 11: Pressure contour for mesh 0 and mesh 1.

4.2.4 The surface pressure coefficient, C_p, distribution

Unlike first-order method, second-order scheme gives mesh 0 and mesh 1 a more similar pressure coefficient distribution. The pinnacle of the pressure coefficient is at the leading edge of the main elements, both meshes gives a very close number(about-5). The second highest spot is at the leading edge of the flap, however, mesh 1 gives the value of it around -4, but mesh 0 gives that around -3.

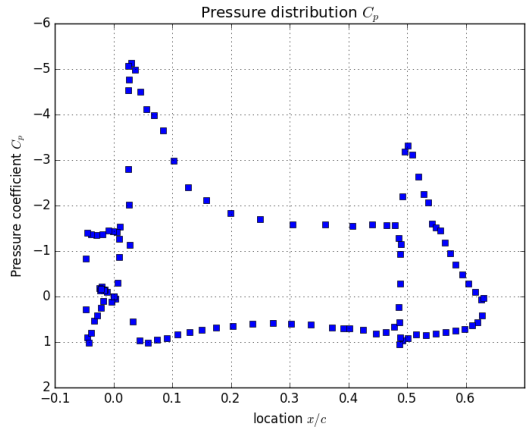

(a) Mesh 0: 1149 elements

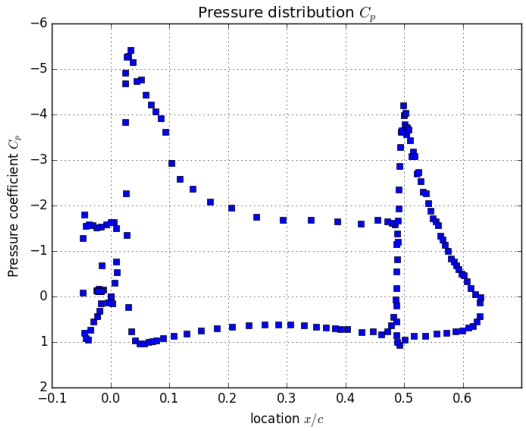

(b) Mesh 1: 2116 elements

fig. 12: Pressure Coefficient C_p contour for mesh 0 and mesh 1.

4.3 Plot the streamlines and calculate the mass flow rate in the slat/main and main/flap gaps.

Figure 7 shows how the air flows over the airfoil, and Table 2 indicates the unit mass flow rate between main/slap and main/flap gaps. Overall, both meshes share a similar streamline pattern and provide the proof that some airflow, indeed, flows through the gaps between airfoil elements, contribute the mass flow rate in Table 2.

(a) mesh 0: 1149 elements

gap location	mass flow rate
slap/main	0.006404
flap/main	0.002313

(b) mesh 1: 2116 elements

gap location	mass flow rate
slap/main	0.006582
flap/main	0.002496

Table 4: Mass flow rate between the main/slap, main/flap gaps, for mesh 0 and mesh 1.

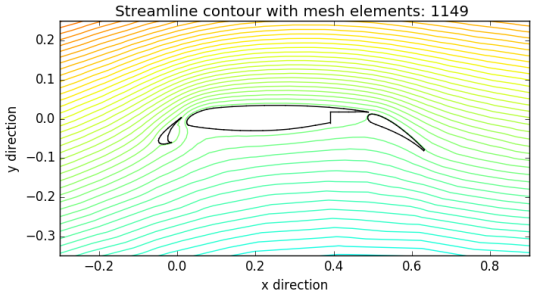

(a) Mesh 0: 1149 elements

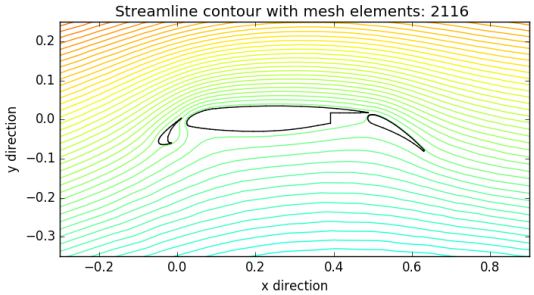

(b) Mesh 1: 2116 elements

fig. 13: Streamline contour for mesh 0 and mesh 1.

5 More Dense Meshes: Mesh 2 and Mesh 3

In this section, more comparison of first order and second order will be discussed.

5.1 mesh 2

5.1.1 Residuals and C_l

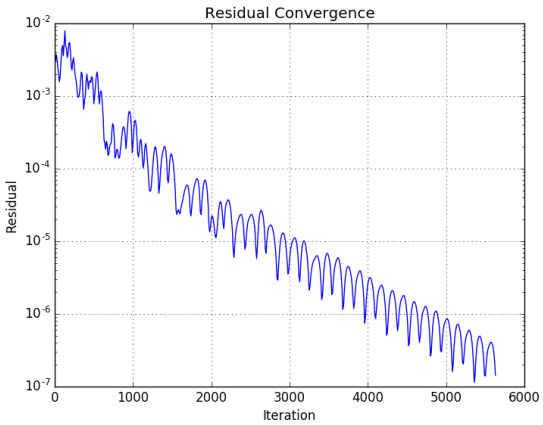

(a) Mesh 0: 1149 elements

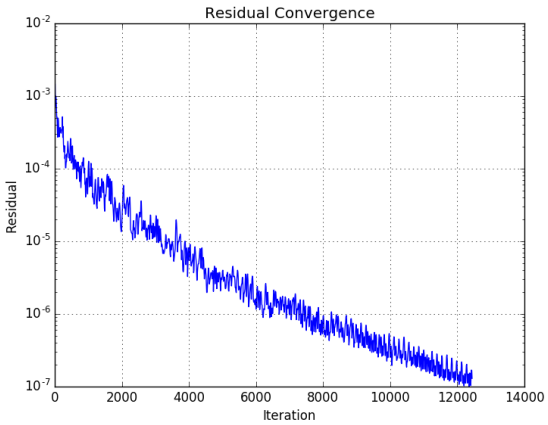

(b) Mesh 1: 2116 elements

fig. 14

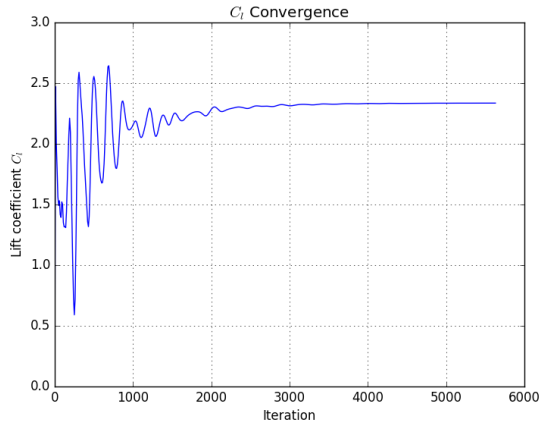

(a) Mesh 0: 1149 elements

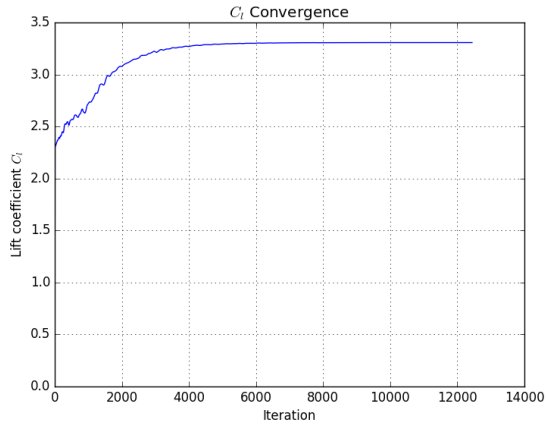

(b) Mesh 1: 2116 elements

fig. 15

5.1.2 The Mach and pressure contours

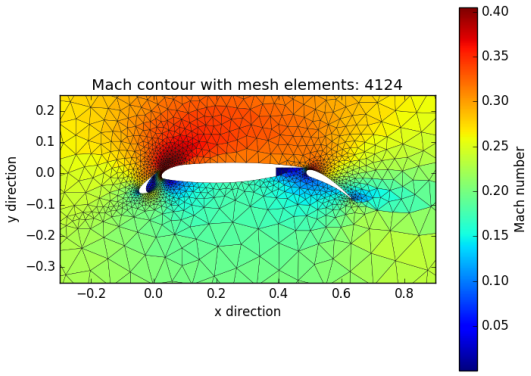

(a) Mesh 0: 1149 elements

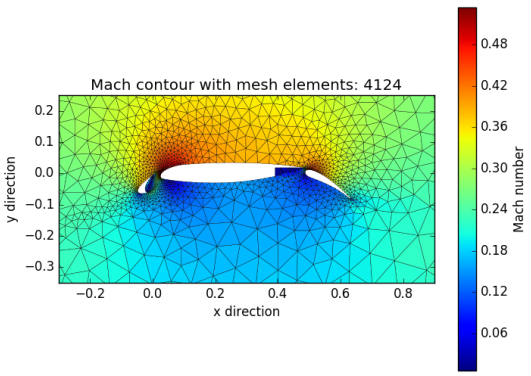

(b) Mesh 1: 2116 elements

fig. 16: Mach number contour for mesh 0 and mesh 1.

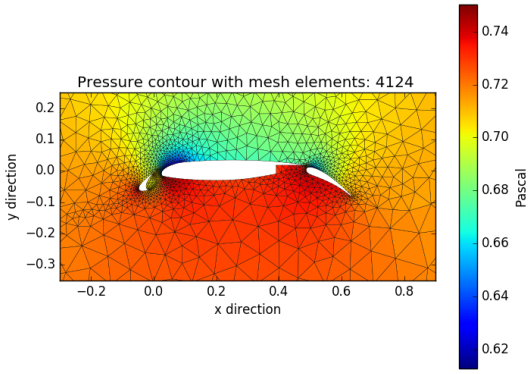

(a) Mesh 0: 1149 elements

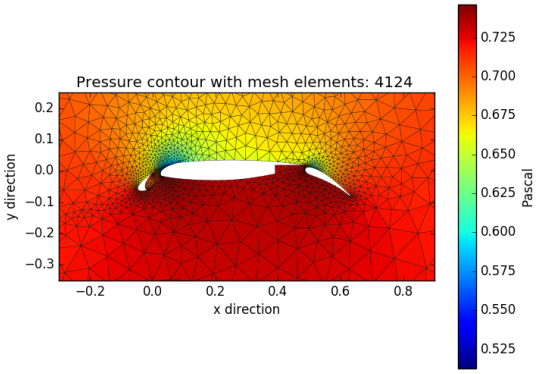

(b) Mesh 1: 2116 elements

fig. 17: Pressure contour for mesh 0 and mesh 1.

5.1.3 The surface pressure coefficient, C_p, distribution

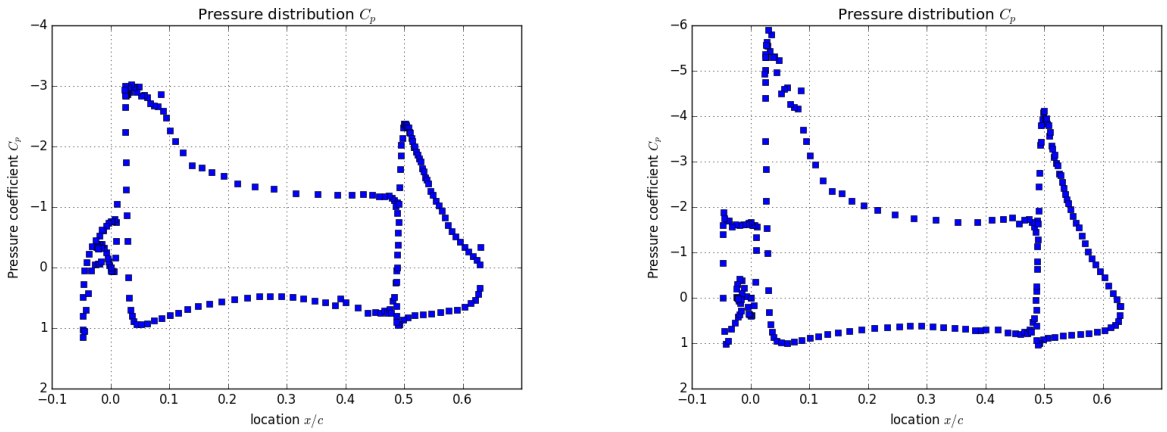

(a) Mesh 0: 4 elements

(b) Mesh 1: 2116 elements

fig. 18: Pressure Coefficient C_p contour for mesh 0 and mesh 1.

5.2 Plot the streamlines and calculate the mass flow rate in the slat/main and main/flap gaps.

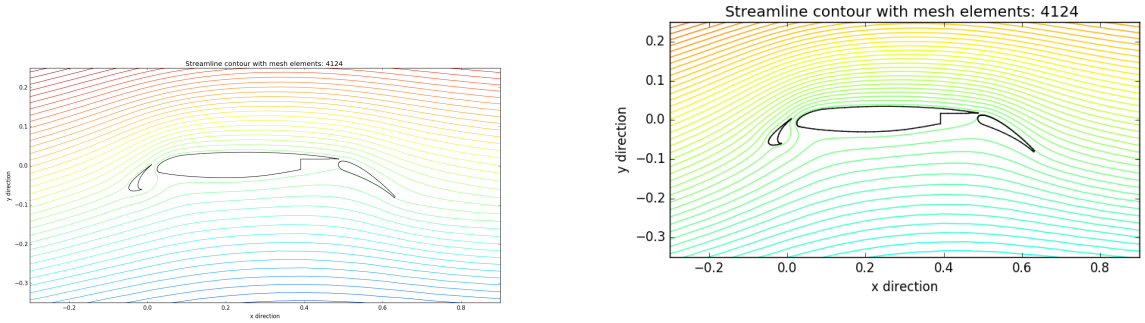

(a) Mesh 0: 1149 elements

(b) Mesh 1: 2116 elements

fig. 19: Streamline contour for mesh 0 and mesh 1.

5.3 mesh 3

Appendix

1. A matrix for uniform grid

```
%=====================Build up the matrices=================================%

for j=1:N+1

    for i=2:N
```

```
        if  j>=2 && j<=N
                m=(j-1)*(N+1)+i;
                r=R0+(i-1)*dr;

                % A matrix
                A(m,m)=-2*(dr^-2+(r*dtheta)^-2);                % Note:
                A(m,m+1)=dr^-2 + (2*r*dr)^-1; % East side       R0+i*dr = r
                A(m,m-1)=dr^-2 - (2*r*dr)^-1; % West side
            A(m,m+(N+1))=(r*dtheta)^-2;  % North side
                A(m,m-(N+1))=(r*dtheta)^-2;  % South side

                % Source term matrix
                q(m)=0;
        end
    end

    %==================Boundary Conditions==========================%
        %hanger
        m=(j-1)*(N+1)+1;q(m,1)=0;
        %farfield
        m=(j-1)*(N+1)+N+1;q(m,1)=R1*sin((j-1)*dtheta);
        %grounds
        q(j,1)=0;m=N*(N+1)+j;q(m,1)=0;
end
```

2. A matrix for compressed grid

Reference

[1] John Anderson: *Computational Fluid Dynamics: The Basics With Applications*, McGraw-Hill 1995.

[2] John Anderson: *Fundamental of Aerodynamics*, McGraw-Hill 2007.

[3] Hirsch,Charles: *Numerical Computation of Internal and External Flows,* vol.I:*Fundamentals of Numerical Discretization,* Wiley, New York, 1988.